AIAA JOURNAL
Vol. 39, No. 8, August 2001

Gap Tones

Christopher K. W. Tam* and Nikolai Pastouchenko†
Florida State University, Tallahassee, Florida 32306-4510

Numerical simulations of the flow and acoustics of a wall jet through a gap using computational aeroacoustics methods are conducted to investigate possible sound generation mechanisms. It is found that discrete frequency sound or tone can be generated by the flow. The tone is produced by the periodic shedding of vortices at the nozzle lip. The vortex shedding process is linked to an acoustic feedback loop. The feedback process appears to begin with the shedding of a vortex at the nozzle lip. A byproduct of the vortex shedding process is the generation of an acoustic pulse. Part of the acoustic pulse propagates across the jet flow and impinges on the wall on the opposite side of the jet. Upon reflection and on propagating through the wall jet in the reversed direction, the sound pulse strikes the nozzle lip. This triggers the shedding of a new vortex accompanied by the generation of a new acoustic pulse. This process repeats itself, and in this way the feedback is closed. A tone frequency prediction formula is derived based on the observed feedback loop. This tone frequency formula appears to be able to provide predictions that are in reasonably good agreement with experimental measurements in a number of cases involving flows through the gaps of multielement high-lift systems.

I. Introduction

IN this study numerical simulation by computational aeroacoustics (CAA) methods is used to investigate possible tone generation mechanisms associated with wall jet type flow through a gap (see Fig. 1). In recent years there have been significant advances in the development of CAA methodology.[1,2] High-order, high-resolution schemes[3,4] are now available. Good quality radiation, inflow and outflow boundary conditions have also been successfully developed.[5] Recently, these CAA methods were employed to simulate the jet screech phenomenon[6,7] and the microfluid flowfields of resonant acoustic liners.[8] In the case of screeching jets, the simulated tone intensity, frequency, the staging phenomenon as well as the jet temperature and nozzle lip thickness effects are found to agree well with experimental measurements. In the case of acoustic liners, most of the acoustic dissipation takes place around the openings of the holes of the face sheet. However, the diameter of the holes is very small (1 mm or less). Thus the flowfield is too small in size for detailed experimental measurements using conventional methods. Numerical simulation provides, for the first time, a clear picture of the flowfield and the mechanisms by which sound waves are absorbed. It turns out that the observed dissipation mechanism is quite different from the classical semi-empirical model, widely used in the acoustic liner community. In this work the same high-quality numerical simulation method is used to investigate the mechanism responsible for producing the gap tones.

In aeroacoustics, tones are often generated by jets and free shear-layer flows. Some of the well-known aeroacoustic tones are the edge tones,[9,10] the screech tones of imperfectly expanded supersonic jets,[11–14] cavity tones,[15,16] jet impingement tones,[17–19] and tones from laminar airfoils.[20,21] All of these tones are generated by an acoustic feedback. In many of these cases, the tone frequency is determined by the requirement that the total phase change around the feedback loop must be an integral number of 2π or the total time taken to go around the loop once must be an integral number of the tone period. In the present investigation of flow through a gap, it is observed that a tone is emitted from nozzle lip region of the wall jet. This is quite unexpected. A closer study reveals that the tone is driven by an acoustic feedback loop. Details of the feedback will be reported later in this paper. Based on repeated observations of the simulated flow and acoustic field, a model of the feedback phenomenon is developed. By means of this model, a tone frequency prediction formula is derived. The predicted frequencies are found to be in good agreement with the measured frequencies of the numerical simulations.

One of the original objectives of this investigation is to explore, through numerical simulation, possible noise sources associated with the flow through the gaps of a high-lift system, such as that shown in Fig. 2. For a three-element airfoil system in the landing configuration, there is a strong wall-jet-like flow through the gap between the slat and the main wing and the gap between the wing and the flap. The present work is, however, exploratory in nature. It is not the intention of this investigation to incorporate all of the flow and geometrical details existing in the gap of a practical high-lift system in the simulations. Only a generic wall jet model as shown in Fig. 1 is used. In adopting a simplified model, only the essential physics are retained. The effects of many flow parameters, such as the boundary-layer thickness on the top and bottom side of the trailing edge of the slat for the front gap or of the main wing for the rear gap, the curvature of the wing or flap below the gap, on the noise generation process would be lost. Any parametric variation study beyond the Mach number M_1 of the wall jet flow, the freestream Mach number M_2, and the gap height H requires the incorporation of the exact geometry of the gap region and the flow conditions. This is beyond the scope of the present investigation.

Recently, Khorrami et al.[22] reported the observation of a strong tone associated with the flow past a three-element energy efficient transport high-lift configuration in a series of experiments conducted in the Low Turbulence Pressure Wind Tunnel at the NASA Langley Research Center. By changing the slat deflection angle, it was found that a lower deflection angle could cause the tone intensity to diminish. It disappeared at very low slat angle setting. Khorrami et al. attributed the source of the tone to be in the gap region between the slat and the main wing near the trailing edge of the slat.

Earlier, Meadows et al.[23] measured the noise emitted from a wing-flap configuration in the Quiet Flow Facility at the Langley Research Center. In this experiment the high-lift system had no slat. However, there was a gap between the wing and the flap. Their measurements showed the presence of a strong tone superimposed on a broadband noise spectrum. Although a parametric study was carried out in the experiment, it was not possible to identify the origin and the generation process of the tone.

In this work an attempt is made to see if the tones observed in the preceding experiments are similar to the gap tones found in the present numerical simulations. For this purpose the tone frequency prediction formula of the present work is used to calculate the tone frequencies of these experiments. In Sec. V of this paper, it will be shown that good agreements are found. It must be emphasized that the good agreement does not constitute a solid proof that the present

Received 11 February 2000; revision received 16 February 2001; accepted for publication 9 March 2001.

*Robert O. Lawton Distinguished Professor, Department of Mathematics. Fellow AIAA.
†Graduate Student, Department of Mathematics.

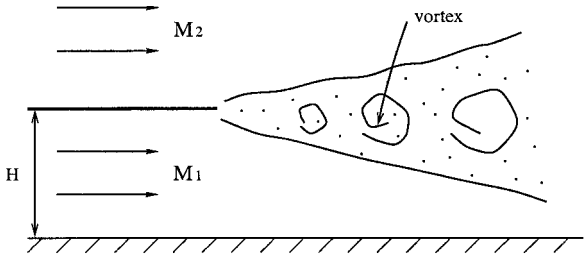

Fig. 1 Generic wall jet model.

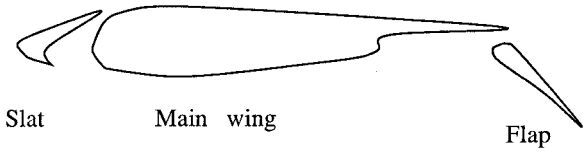

Fig. 2 Three-element high-lift system in landing configuration.

gap tone generation mechanism is responsible for the tones of these experiments. However, it does suggest that an acoustic feedback could play an important role in their generation.

In Sec. II a generic wall jet model of the gap flow between the slat and the main wing or the main wing and the flap is described. This is followed by a description of the computation model and numerical algorithm used to simulate the flow and acoustic fields of the wall jet. In Sec. III the observation of a feedback loop responsible for the generation of gap tones is reported. A mathematical model of the feedback loop is then formulated in Sec. IV. Based on this model, a gap tone frequency prediction formula is derived. It will be shown that the predicted tone frequencies agree well with experimental measurements. The relevance of the observed gap tone feedback mechanism to airframe tones will be briefly discussed in the conclusion of this paper.

II. Wall Jet Model

The geometry of a high-lift wing system (Fig. 2) is quite complicated. It is our belief that the basic gap tone generation mechanism is quite independent of the detailed geometry of the slat, wing, and flap. The fundamental fluid mechanical processes can be found, even if a somewhat simplified gap flow model is used. In this work a generic wall jet model representative of both of the slat gap and the flap gap flow is employed.

Experimental measurements and Reynolds-averaged Navier–Stokes computations indicate that there is a high velocity flow in the slat gap as well as the flap gap. Each of these high-speed flows emerges as a wall jet at the gap exit. The wall jet attaches to the upper surface of the main wing in the case of the slat gap and the flap in the case of the flap gap. Outside the wall jet is an ambient stream of fluid moving at a lower speed. A mixing layer develops downstream of the trailing edge of the slat or the main wing separating the wall jet and the ambient flow.

Figure 1 shows the generic two-dimensional wall jet model to be used in the present numerical simulation. A two-dimensional model should be adequate as the aspect ratio of the slat or flap gap is very large. In the model the wall jet of the slat or flap gap flow is represented by a wall jet of Mach number M_1 over a plane wall. The bottom wall of Fig. 1 models the upper surface of the main wing in the case of the slat gap and that of the flap in the case of the flap gap. The channel from which the wall jet emerges (Fig. 1) is formed by a zero thickness flat plate placed at a distance of H from the plane wall. The thin flat plate models the trailing edge of the slat or the main wing (Fig. 2). For simplicity, the outside flow will be assumed to be uniform at a Mach number $M_2 (M_1 > M_2)$. Downstream of the trailing edge of the flat plate, a mixing layer is formed. Here large vortical structures, the well-known Brown–Roshko structures, would develop and persist over a long distance downstream.

III. Computation Model and Numerical Algorithm

The wall jet model of Fig. 1 is used in the present investigation to identify possible mechanisms by which tones are generated. This is accomplished by numerical simulation. Basically, the gap flow and acoustic field are computed by a time-marching algorithm. When tones are found, the processes by which they are generated are then identified in the simulation.

A. Computation Model

Figure 3 shows the computation domain used in the simulations. To ensure that this choice of the computation domain is adequate, some runs were repeated using a smaller size domain. It became clear that the frequencies and intensities of the gap tones found were not affected by the size reduction. We believe that the tone phenomenon observed in the simulation, which will be reported in the next section, is adequately resolved by the computation domain of Fig. 3. No larger size domain is necessary.

For a high-lift wing system the mixing layer between the wall jet of the slat or flap gap and the ambient fluid is turbulent. To simulate the effect of turbulence, here the k–ε turbulence model is employed. For convenience, dimensionless variables with respect to length scale $= H$ (the gap height), velocity scale $= a_\infty$ (ambient sound speed), timescale $= H/a_\infty$, density scale $= \rho_\infty$ (ambient gas density), pressure scale $= \rho_\infty a_\infty^2$ and molecular kinematic viscosity scale $= Ha_\infty$ are used. The governing equations including the k–ε model are

$$\frac{\partial \rho}{\partial t} + \frac{\partial \rho u}{\partial x} + \frac{\partial \rho v}{\partial y} = 0 \tag{1}$$

$$\rho\left(\frac{\partial u}{\partial t} + u\frac{\partial u}{\partial x} + v\frac{\partial u}{\partial y}\right) = -\frac{\partial p}{\partial x} + \frac{\partial(\rho\sigma_{xx})}{\partial x} + \frac{\partial(\rho\sigma_{xy})}{\partial y} \tag{2}$$

$$\rho\left(\frac{\partial v}{\partial t} + u\frac{\partial v}{\partial x} + v\frac{\partial v}{\partial y}\right) = -\frac{\partial p}{\partial y} + \frac{\partial(\rho\sigma_{yx})}{\partial x} + \frac{\partial(\rho\sigma_{yy})}{\partial y} \tag{3}$$

$$\frac{\partial p}{\partial t} + u\frac{\partial p}{\partial x} + v\frac{\partial p}{\partial y} + \gamma p\left(\frac{\partial u}{\partial x} + \frac{\partial v}{\partial y}\right) = 0 \tag{4}$$

$$\rho\left(\frac{\partial k}{\partial t} + u\frac{\partial k}{\partial x} + v\frac{\partial k}{\partial y}\right) = \rho\sigma_{ij}\frac{\partial u_i}{\partial x_j} - \rho\varepsilon + \frac{1}{\sigma_k}\left[\frac{\partial}{\partial x}\left(\rho\nu_t\frac{\partial k}{\partial x}\right) + \frac{\partial}{\partial y}\left(\rho\nu_t\frac{\partial k}{\partial y}\right)\right] \tag{5}$$

$$\rho\left(\frac{\partial \varepsilon}{\partial t} + u\frac{\partial \varepsilon}{\partial x} + v\frac{\partial \varepsilon}{\partial y}\right) = c_{\varepsilon 1}\frac{\varepsilon}{k+k_0}\rho\sigma_{ij}\frac{\partial u_i}{\partial x_j} - c_{\varepsilon 2}\frac{\rho\varepsilon^2}{k+k_0} + \frac{1}{\sigma_\varepsilon}\left[\frac{\partial}{\partial x}\left(\rho\nu_t\frac{\partial \varepsilon}{\partial x}\right) + \frac{\partial}{\partial y}\left(\rho\nu_t\frac{\partial \varepsilon}{\partial y}\right)\right] \tag{6}$$

where

$$\nu_t = c_\mu\frac{k^2}{\varepsilon + \varepsilon_0} + \nu \tag{7}$$

$$\sigma_{ij} = \nu_t\left(\frac{\partial u_i}{\partial x_j} + \frac{\partial u_j}{\partial x_i} - \frac{2}{3}\frac{\partial u_k}{\partial x_k}\delta_{ij}\right) - \frac{2}{3}k\delta_{ij} \tag{8}$$

The turbulence intensity k and stresses σ_{ij} are nondimensionalized by a_∞^2. The dissipation rate ε is nondimensionalized by a_∞^3/H. We will use the numerical values of the various constants given by Thies and Tam.[24] These constants are found specifically for free shear flows. The numerical values are

$$c_\mu = 0.0874, \qquad c_{\varepsilon 1} = 1.4, \qquad c_{\varepsilon 2} = 2.02$$

$$\sigma_k = 0.327, \qquad \sigma_\varepsilon = 0.377, \qquad \nu = 2 \times 10^{-6}$$

The two quantities k_0 and ε_0 are inserted into Eqs. (6) and (7) to prevent division by zero. In the present computation they are set equal to 10^{-6} and 10^{-4}, respectively.

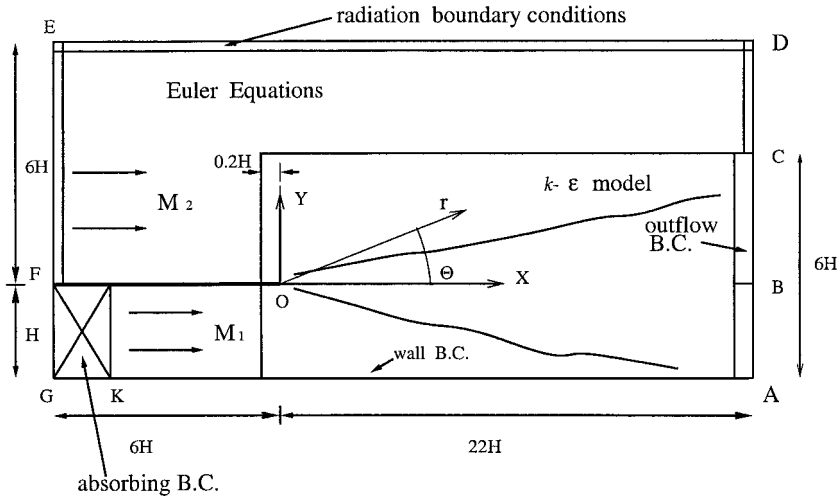

Fig. 3 Computation domain.

In the computation Eqs. (1–8) are applied to the lower right-hand region of the computation domain as shown in Fig. 3. Outside this region turbulence and viscosity are unimportant. In the outside regions the governing equations are the Euler equations

$$\frac{\partial \rho}{\partial t} + \frac{\partial \rho u}{\partial x} + \frac{\partial \rho v}{\partial y} = 0 \tag{9}$$

$$\rho\left(\frac{\partial u}{\partial t} + u\frac{\partial u}{\partial x} + v\frac{\partial u}{\partial y}\right) = -\frac{\partial p}{\partial x} \tag{10}$$

$$\rho\left(\frac{\partial v}{\partial t} + u\frac{\partial v}{\partial x} + v\frac{\partial v}{\partial y}\right) = -\frac{\partial p}{\partial y} \tag{11}$$

$$\frac{\partial p}{\partial t} + u\frac{\partial p}{\partial x} + v\frac{\partial p}{\partial y} + \gamma p\left(\frac{\partial u}{\partial x} + \frac{\partial v}{\partial y}\right) = 0 \tag{12}$$

B. Computation Schemes

Equations (1–12) are discretized according to the seven-point stencil dispersion-relation-preserving (DRP) scheme.[3] The DRP scheme was designed to solve CAA problems in the time domain. The scheme uses central difference quotient with optimized coefficients. It has no numerical dissipation and little dispersion (for waves with wavelengths equal to or longer than seven mesh spacings) and is well suited for capturing small-amplitude acoustic disturbances. Near a boundary where a seven-point central difference stencil does not fit, backward difference stencils are used. The stencil coefficients are given in Ref. 1. Throughout this work a square mesh with $\Delta x = \Delta y = H/50$ is used. The time step Δt is taken to be 0.001. This is much smaller than that required by numerical stability. But it allows a more precise determination of the tone frequencies for comparisons with theoretical values.

C. Numerical Boundary Conditions

A set of high-quality numerical boundary conditions is essential to the present simulations. These boundary conditions must allow acoustic and flow disturbances to leave the computation domain with little or no reflection. Recently an in-depth review of this subject is given in Ref. 5. For the present problem the Tam and Webb[3] radiation and outflow boundary conditions with a slight modification for the presence of a wall are used. Along boundary CDE of Fig. 3, the following radiation boundary conditions are imposed:

$$\frac{1}{V_2(\theta)}\frac{\partial}{\partial t}\begin{bmatrix}\rho\\ u\\ v\\ p\end{bmatrix} + \left(\cos\theta\frac{\partial}{\partial x} + \sin\theta\frac{\partial}{\partial y}\right)\begin{bmatrix}\rho\\ u\\ v\\ p\end{bmatrix} + \frac{1}{2r}\begin{bmatrix}\rho - 1\\ u\\ v\\ p - 1/\gamma\end{bmatrix} = 0 \tag{13}$$

where (r, θ) are the polar coordinates and $V_2(\theta) = M_2\cos\theta + (1 - M_2^2\sin^2\theta)^{\frac{1}{2}}$. M_2 is the Mach number of the ambient flow, and γ is the ratio of the specific heats of the gas.

Along boundary EF, there is a uniform inflow at Mach M_2. At the same time there are outgoing acoustic waves. To generate the inflow and to allow the outgoing acoustic disturbances to leave smoothly, the physical variables are split up into two parts,

$$\begin{bmatrix}\rho\\ u\\ v\\ p\end{bmatrix} = \begin{bmatrix}1\\ M_2\\ 0\\ 1/\gamma\end{bmatrix} + \begin{bmatrix}\rho'\\ u'\\ v'\\ p'\end{bmatrix}$$

The first part is the incoming mean flow. The second part is the outgoing acoustic waves. The outgoing acoustic waves satisfy boundary condition (13). The variables are updated in time by Eq. (13) in the same way as those along boundary CDE.

Along boundary BC the following modified Tam and Webb[3] outflow boundary conditions are used:

$$\frac{\partial \rho}{\partial t} + u\frac{\partial \rho}{\partial x} = \frac{\partial p}{\partial t} + u\frac{\partial p}{\partial x} \tag{14}$$

$$\frac{\partial u}{\partial t} + u\frac{\partial u}{\partial x} = -\frac{\partial p}{\partial x} \tag{15}$$

$$\frac{\partial v}{\partial t} + u\frac{\partial v}{\partial x} = -\frac{\partial p}{\partial y} \tag{16}$$

$$\frac{1}{V(\theta)}\frac{\partial p}{\partial t} + \cos\theta\frac{\partial p}{\partial x} + \sin\theta\frac{\partial p}{\partial y} + \left(p - \frac{1}{\gamma}\right)\frac{1}{2r} = 0 \tag{17}$$

$$\frac{\partial k}{\partial t} + u\frac{\partial k}{\partial x} = 0 \tag{18}$$

$$\frac{\partial \varepsilon}{\partial t} + u\frac{\partial \varepsilon}{\partial x} = 0 \tag{19}$$

where $V(\theta) = u\cos\theta + (1 - u^2\sin^2\theta)^{\frac{1}{2}}$. Boundary conditions (14–19) are essentially the same used by Shen and Tam[6] in their screeching jet simulations. In the present problem the velocity component v is small and has been dropped from the equations. Along boundary AB outflow boundary conditions (14–19), except (17), are again used. To avoid excessive reflection of acoustic disturbances from the corner region near A because of the presence of the wall, Eq. (17) is replaced by the following equation:

$$\frac{1}{\bar{V}(\theta)}\frac{\partial p}{\partial t} + \frac{\partial p}{\partial x} + \left(p - \frac{1}{\gamma}\right)\frac{1}{2x} = 0 \tag{20}$$

where $\bar{V}(\theta) = 1 + u$. The change from Eqs. (17–20) takes into account the presence of the wall AK. Because of the wall, the acoustic disturbances propagate essentially in the x direction as nearly plane waves.

On the wall surfaces the wall boundary condition is enforced by means of the ghost point method. Details of the ghost point method can be found in Ref. 25 and will not be elaborated upon here.

D. Duct Termination Condition

The space between the flat plate OF and the wall AG of Fig. 3 forms a ducted region in which acoustic waves propagating obliquely toward the boundary FG would be reflected back and forth by the two walls. To minimize the reflection of acoustic disturbances back into the computation domain, a special set of duct termination conditions is imposed at the end of the ducted region. We found, after some experimentation, that a length of $2H$ is quite adequate for this region.

In the duct termination region the flow variables are divided into two parts, i.e.,

$$\begin{bmatrix} \rho \\ u \\ v \\ p \end{bmatrix} = \begin{bmatrix} 1 \\ M_1 \\ 0 \\ 1/\gamma \end{bmatrix} + \begin{bmatrix} \rho_0 \\ u_0 \\ v_0 \\ p_0 \end{bmatrix} \tag{21}$$

where the first term of Eq. (21) is the steady incoming mean flow. M_1 is the Mach number of the wall jet. The second term is the outgoing acoustic disturbances. To avoid reflection back into the computation domain, the outgoing disturbances are to be damped out before they reach the outer boundary FG by adding a frictional damping term to the governing equations. These equations are

$$\begin{aligned} &\frac{\partial \rho_0}{\partial t} + M_1 \frac{\partial \rho_0}{\partial x} + \frac{\partial u_0}{\partial x} + \frac{\partial v_0}{\partial y} = -\frac{1}{R_d}\rho_0 \\ &\frac{\partial u_0}{\partial t} + M_1 \frac{\partial u_0}{\partial x} = -\frac{\partial p_0}{\partial y} - \frac{1}{R_d}u_0 \\ &\frac{\partial v_0}{\partial t} + M_1 \frac{\partial v_0}{\partial x} = -\frac{\partial p_0}{\partial y} - \frac{1}{R_d}v_0 \\ &\frac{\partial p_0}{\partial t} + M_1 \frac{\partial p_0}{\partial x} + \left(\frac{\partial u_0}{\partial x} + \frac{\partial v_0}{\partial y}\right) = -\frac{1}{R_d}p_0 \end{aligned} \tag{22}$$

The inverse frictional Reynolds number R_d^{-1} is chosen to have the form

$$\frac{1}{R_d} = \begin{cases} \frac{1}{2}F_{\max}\{1 - \cos[(x_G + 2 - x)\pi]\}, & x_G + 1 \le x \le x_G + 2 \\ F_{\max} = (1 - M_1)3\,\ell n(10), & x_G \le x < x_G + 1 \end{cases} \tag{23}$$

where x_G is the x location of the point G. Equation (23) provides a smooth frictional damping. The smoothness reduces back reflection into the computation domain.

Because a seven-point stencil is used, some stencils, which originate from the duct termination region, extend outside the region into the channel region of the computation domain. In the computation domain the variables are computed by Eqs. (9–12). They are (ρ, u, v, p). To obtain the values of (ρ_0, u_0, v_0, p_0) at these points so that Eqs. (22) can be used, one can make use of Eq. (21). The same treatment applies to stencils that extend from the computational domain into the duct termination region.

E. Artificial Selective Damping

The DRP scheme is a central difference scheme and, therefore, has no intrinsic numerical damping. To eliminate spurious short waves, artificial selective damping[26] is added to the discretized governing equations. The distribution of artificial selective damping follows the design of Ref. 6. In the interior region general background damping using the seven-point damping stencil (with half-width $\sigma = 0.2\pi$) is enforced. The inverse mesh Reynolds number $R_\Delta^{-1} = \nu_a/(a_\infty \Delta)$, where ν_a is the artificial kinematic viscosity and Δ is the mesh spacing, is assigned the numerical value of 0.05. Along the boundaries of the computation domain and wall surfaces, wherever the seven-point damping stencil does not fit, smaller damping stencils[1] are used. The inverse mesh Reynolds number has a distribution in the form of a Gaussian with a half-width of four mesh points (normal to the boundary). The maximum of the Gaussian is on the boundary with an assigned value of 0.15.

At the lip of the wall jet, the point O in Fig. 3, extra damping is required. The following Gaussian distribution of R_Δ^{-1} around this point has been found to give satisfactory results:

$$R_\Delta^{-1} = 0.8 \exp\{-(\ell n 2)[(x^2 + y^2)/16\Delta^2]\} \tag{24}$$

IV. Numerical Simulations and Observations

A large number of numerical simulations of the wall jet flow and acoustic fields were carried out. The initial conditions used for all of the simulations were

$$t = 0, \qquad u = M_2, \qquad v = 0, \qquad \rho = 1, \qquad p = 1/\gamma \tag{25}$$

In the duct termination region there were no outgoing disturbances at the beginning. The null initial conditions were used, i.e.,

$$u_0 = v_0 = \rho_0 = p_0 = 0 \tag{26}$$

After careful observations of the computed results of many simulations, it becomes clear that the wall jet, with or without ambient flow, emits a gap tone near the trailing edge of the flat plate at O of Fig. 3 or the nozzle lip of the wall jet. The sound is generated by the shedding of vortices at the nozzle lip. The vortex shedding process is regulated in time by a feedback loop. The entire sound generation process including the feedback loop can be seen in Fig. 4. Figure 4a shows the density field of the left half of the computation domain. In this figure the flat wall forms the bottom of the figure. The zero thickness plate that separates the channel flow and the ambient gas is shown as the line of discontinuity on the bottom-left-hand side of the figure. Above the thin plate acoustic waves in the form of concentric circular arcs radiating from the trailing edge of the plate can be seen. Downstream of the trailing edge, large vortical structures can be found in the mixing layer formed by the wall jet and ambient fluid. In Fig. 4a near the trailing edge a vortex has just been shed. Accompanying the shedding of the vortex, an acoustic pulse is generated. Half the pulse propagates into the upper half plane. This is seen as the white band near the trailing edge of the plate. The other half propagates down through the wall jet flow. The sound waves are seen as the curved, alternately black and white, bands. The bands appear to have the nozzle lip or trailing edge of the thin plate as the apparent center.

Figures 4b–4d show the evolution of the acoustic and flowfield in time. Figure 4b, at a later time than Fig. 4a, shows that the acoustic pulse in the wall jet, which in the preceding figure propagate toward the wall, has been reflected back by the wall. The sound pulse now propagates toward the mixing layer and the nozzle lip. Figure 4c shows the instant when the reflected pulse strikes the nozzle lip of the wall jet leading to the shedding of the another vortex. The shedding of a new vortex leads to the emission of another acoustic pulse as shown in Fig. 4d. The cycle now repeats itself.

In Fig. 4 the simulation was carried out without ambient flow. But other simulations indicated that the feedback vortex shedding phenomenon remains the same even when there is an outside flow at Mach M_2. Measured tone frequencies, however, are found to be almost unaffected by the outside flow.

V. Tone Frequency Formula and Comparisons with Experiments

In this section a frequency formula for the gap tones based on the preceding observed feedback loop is derived. The tone frequencies calculated by this formula are then compared with the measured tone frequencies in numerical simulations and physical experiments.

A. Tone Frequency Prediction Formula

Figure 5a shows schematically the feedback loop of the gap tone. Sound generated by the vortex shedding process (a pulse of sound) propagates across the wall jet. Upon impinging on the wall, it is

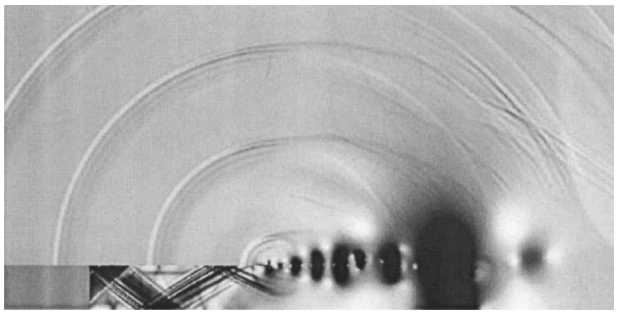

a) $t = 15.75$

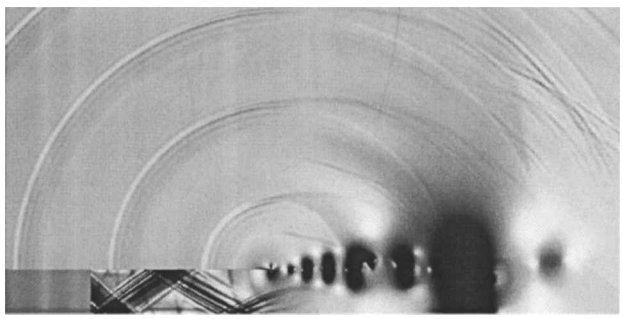

b) $t = 16.75$

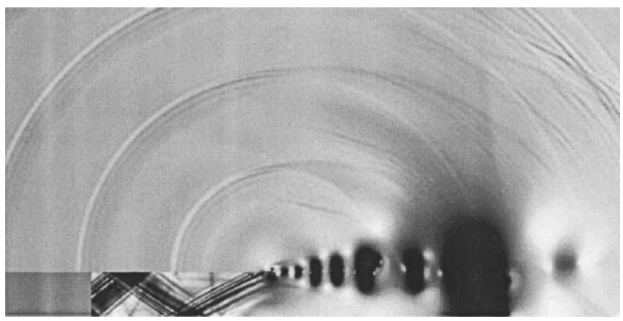

c) $t = 17.50$

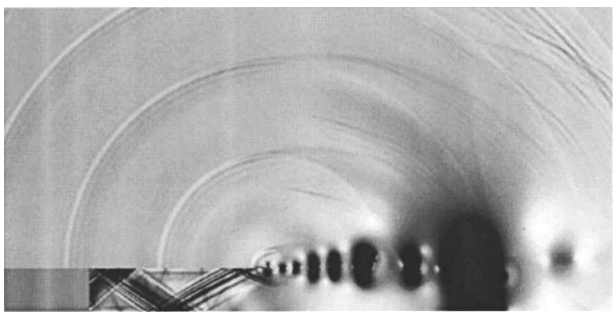

d) $t = 17.75$

Fig. 4 Density field of simulated wall jet flow and acoustic fields showing the generation of a gap tone and large vortical structures in the upper mixing layer: $M_1 = 0.4$, $M_2 = 0.0$.

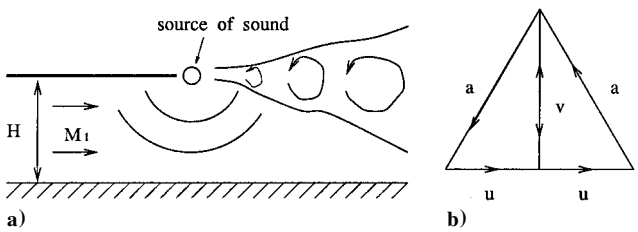

Fig. 5 Feedback loop and the velocity vector diagram.

reflected back. Propagating through the wall jet, the reflected sound strikes the nozzle lip. This triggers the shedding of a new vortex and the generation of another sound pulse. This closes the feedback loop.

Figure 5b shows the velocity diagram of the sound waves. In propagating across the wall jet toward the wall on the other side, the acoustic ray must point upstream so that the component in the flow direction exactly cancels out the convection velocity of the jet flow u. This is illustrated on the left half of the velocity vector diagram. Let the sound speed be a, then the propagation velocity normal to the wall is given by

$$v = (a^2 - u^2)^{\frac{1}{2}} \tag{27}$$

On following the same reasoning, it is easy to conclude that the cross-stream velocity of the reflected wave that hits the nozzle lip is also given by Eq. (27). The velocity vectors involved are shown on the right half of Fig. 5b. Because the gap height is H, the time of travel around the feedback loop is $2H/v$ plus a small delay time Γ (time delay between the time the sound waves striking the nozzle trailing edge and the shedding of a vortex). But if T is the period of oscillation, the time of travel over the feedback loop must be equal to an integral number of T. This yields

$$2H\Big/(a^2 - u^2)^{\frac{1}{2}} + \Gamma = nT, \qquad \text{where} \qquad n = 1, 2, 3, \ldots$$

In his study of the cavity tone feedback loop, Rossiter[15] also included a time-delay term in his famous formula. Obviously Γ depends on the boundary-layer thickness at the trailing edge of the wall jet. However, for thin boundary layer Γ is quite small. Here as a first approximation it will be neglected. Thus the frequency of the gap tone f is given by

$$f = n(a^2 - u^2)^{\frac{1}{2}}\Big/2H, \qquad n = 1, 2, 3, \ldots \tag{28}$$

B. Comparisons with Numerical Simulations

The feedback loop involves primarily the propagation of sound across the wall jet. Therefore, whether there is an ambient flow outside the wall jet or not would not affect appreciably the frequency formula (28). To test both the accuracy of (28) and its independence of ambient flow speed, a series of numerical simulations was carried out with different wall jet Mach number M_1 and ambient flow Mach number M_2 ($M_1 > M_2$). Figure 6 shows comparisons between the measured tone frequencies and those calculated by Eq. (28) for M_1 up to 0.4 and M_2 up to 0.3. As can be seen, the measured frequencies are, for all intents and purposes, independent of M_2 and agree well with formula (28).

C. Comparisons with Physical Experiments

In a recent airframe noise experiment[22,27] involving a three-element high-lift wing model in the Low Turbulence Pressure

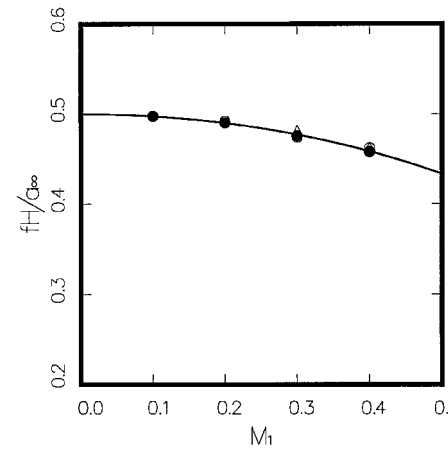

Fig. 6 Comparisons between tone frequencies measured in numerical simulations and calculated by Eq. (28): ●, $M_2 = 0.0$; ○, $M_2 = 0.1$; △, $M_2 = 0.2$; ◇, $M_2 = 0.3$; and ——, theory.

Tunnel at the NASA Langley Research Center, a strong tone was detected. The tone was found to be emitted from the gap region between the slat and the main wing. The tone frequency centered around 50 kHz. The gap height H was 1.35 cm. Now if we use a (speed of sound) = 340 m/s, $u = 0.25a$ and $n = 4$, formula (28) gives a tone frequency of 48.8 kHz. This is very close to the observed frequency. Reference 22 reported a slight decrease of the tone frequency when there is a reduction in the flow Reynolds number or a thickening of the trailing-edge boundary layer. For simplicity the time-delay term Γ was neglected in deriving Eq. (28). For a thick boundary layer Γ is larger. If this effect is included in calculating the tone frequency, it will lead to a slight frequency drop consistent with experimental observation.

In Ref. 23 the noise of a two-element wing-flap combination was measured in the NASA Langley Research Center Quiet Flow Facility. At a flight speed of Mach 0.17, a strong tone was detected at a frequency around 49 kHz. By using the gap height H of 1.02 cm provided in Ref. 23 and taking $a = 340$ m/s, $u = 0.25a$ and $n = 3$, formula (28) gives a gap tone frequency of 48.4 kHz. This is in good agreement with the measured value. Data at a lower Mach number 0.15 indicate a slight downshift of the tone frequency. We believe this shift is similar to the frequency shift caused by the thickening of the boundary layer at the slat trailing edge as just discussed. The reason for the frequency drop is the same.

Reference 28 reported the observation of significant amount of slat gap noise over the frequency band of 12–20 kHz. The exact mechanism responsible for producing this noise component was not known. Now, let us assume that the noise was related to gap tones. The slat gap had a height of 1.676 cm (0.66 in.). If we take $u = 0.5a$, $n = 2$ and $a = 340$ m/s, formula (28) yields a tone frequency of 17.5 kHz. The measured spectrum has a main peak at 15 kHz and a minor peak at 17 kHz. The wing surface is curved in the slat gap region so that the effective gap height for the feedback loop may not be precisely the minimum height (0.66 in.). In other words, the predicted gap tone frequency of formula (28) is not too far off to rule out the feedback mechanism as a possible contributing factor to the measured slat gap noise.

VI. Conclusions

In this work we report the discovery, using numerical simulation, of a feedback mechanism by which gap tones are generated. The tones are produced by the vortex shedding process at the lip of the wall jet. The vortex shedding process is maintained by a feedback loop. The feedback loop controls the frequency of the tone. The feedback consists of the emission of a sound pulse as a vortex is shed at the lip of the wall jet. Part of the sound waves propagate across the wall jet and impinge on the wall on the other side. Upon reflection from the wall, the reflected sound wave, now propagating in the opposite direction, excites the shear layer when impinging on the nozzle lip. This causes the shedding of a new vortex and the generation of a new acoustic pulse. The process then repeats itself.

In their study of flow around a three-element high-lift wing system, Khorrami et al.[22] proposed that vortex shedding associated with flow past the blunt trailing edge of the slat was the source of tones. It is well known that blunt trailing edge facilitates vortex shedding. There is no doubt from their work that sound did produce by the vortex shedding process as they have proposed. The blunt trailing-edge tone generation mechanism, however, does not readily yield a single tone frequency formula that can be used to compare with experimental measurements. In an earlier report of their work, Khorrami et al.[27] reported that efforts to correlate the vortex shedding frequency to the thickness of the blunt trailing edge were not successful. Attempts to correlate the frequency with the displacement thickness δ^* of the wall boundary layer were then made. But the displacement thickness on the two sides of the slat were found to be widely different, because of the large difference Khorrami et al. declared that the proper choice of δ^* was problematic. They offered no definitive conclusion on what determined the vortex shedding frequency.

We believe that if the slat has a blunt trailing edge, vortex shedding in the form found by Khorrami et al. can be the preferred mechanism. However, the shedding frequency might be regulated by the acoustic feedback loop found in the present work rather than the thickness of the blunt trailing edge or the boundary-layer displacement thickness. In other words, the blunt trailing-edge mechanism is assisted by the feedback process.

Finally, we like to point out that the gap tone frequency formula (28) is based purely on kinematic consideration. The integer n in the formula is an unspecified parameter that must be selected somewhat empirically. Dynamically, the choice of the integer n is, however, dictated by the instability characteristics of the trailing-edge flow. Obviously the observed tone frequency would correspond to the value of n for which the gap tone frequency determined by formula (28) is closest to the most unstable frequency of the trailing-edge flow. This is, however, not a trivial problem and is beyond the scope of the present work.

Acknowledgments

C. K. W. Tam wishes to thank the Lockheed Martin Aeronautical Systems Company and the Advanced Subsonic Technology program for providing financial support through Task 1 of NAS1–20102. N. Pastouchenko was supported by NASA Langley Research Center Grant NAG1–2145.

References

[1]Tam, C. K. W., "Computational Aeroacoustics: Issues and Methods," *AIAA Journal*, Vol. 33, No. 10, 1995, pp. 1788–1796.

[2]Lele, S. K., "Computational Aeroacoustics: A Review," AIAA Paper 97-0018, Jan. 1997.

[3]Tam, C. K. W., and Webb, J. C., "Dispersion-Relation-Preserving Finite Difference Schemes for Computational Acoustics," *Journal of Computational Physics*, Vol. 107, 1993, pp. 262–281.

[4]Lele, S. K., "Compact Finite Difference Schemes with Spectral-Like Resolution," *Journal of Computational Physics*, Vol. 103, 1992, pp. 16–42.

[5]Tam, C. K. W., "Advances in Numerical Boundary Conditions for Computational Aeroacoustics," *Journal of Computational Acoustics*, Vol. 6, Dec. 1998, pp. 377–402.

[6]Shen, H., and Tam, C. K. W., "Numerical Simulation of the Generation of Axisymmetric Mode Jet Screech Tones," *AIAA Journal*, Vol. 36, No. 10, 1998, pp. 1801–1807.

[7]Shen, H., and Tam, C. K. W., "Effects of Jet Temperature and Nozzle-Lip Thickness on Screech Tones," *AIAA Journal*, Vol. 38, No. 5, 2000, pp. 762–767.

[8]Tam, C. K. W., and Kurbatskii, K. A., "Microfluid Dynamics and Acoustics of Resonant Liners," *AIAA Journal*, Vol. 38, No. 8, 2000, pp. 1331–1339.

[9]Powell, A., "On the Edgetone," *Journal of the Acoustical Society of America*, Vol. 33, No. 4, 1961, pp. 359–409.

[10]Karamcheti, K., Bauer, A. B., Shields, W. L., Stegen, G. R., and Woolley, J. P., "Some Features of an Edge-Tone Flow field," NASA SP 207, July 1969, pp. 275–304.

[11]Powell, A., "On the Mechanism of Choked Jet Noise," *Proceedings of Physical Society, London*, Vol. 66, 1953, pp. 1039–1056.

[12]Powell, A., "The Noise of Choked Jet," *Journal of the Acoustical Society of America*, Vol. 25, 1953, pp. 385–389.

[13]Tam, C. K. W., Seiner, J. M., and Yu, J. C., "Proposed Relationship Between Broadband Shock Associated Noise and Screech Tones," *Journal of Sound and Vibration*, Vol. 110, 1986, pp. 309–321.

[14]Shen, H., and Tam, C. K. W., "Three-Dimensional Numerical Simulation of the Jet Screech Phenomenon," AIAA Paper 2001-0820, Jan. 2001.

[15]Rossiter, J. E., "Wind Tunnel Experiments of the Flow over Rectangular Cavities at Subsonic and Transonic Speeds," Aeronautical Research Council, R. & M. 3438, 1964.

[16]Tam, C. K. W., and Block, P. J. W., "On the Tones and Pressure Oscillations Induced by Flow over Rectangular Cavities," *Journal of Fluid Mechanics*, Vol. 89, 1978, pp. 373–399.

[17]Wagner, F. R., "The Sound and Flow field of an Axially Symmetric Free Jet upon Impact on a Wall," NASA TT F-13942, 1971.

[18]Neuwerth, G., "Acoustic Feedback of a Subsonic and Supersonic Free Jet Which Impinges on an Obstacle," NASA TT F-15719, 1974.

[19]Tam, C. K. W., and Ahuja, K. K., "Theoretical Model of Discrete Tone Generation by Impinging Jets," *Journal of Fluid Mechanics*, Vol. 214, 1990, pp. 67–87.

[20]Tam, C. K. W., "Discrete Tones of Isolated Airfoils," *Journal of the Acoustical Society of America*, Vol. 55, No. 6, 1974, pp. 1173–1177.

[21]Lowson, M., and Swales, C., "Acoustic Studies on a NACA 0012 Airfoil," AIAA Paper 96-0155, Jan. 1996.

[22]Khorrami, M. R., Berkman, M. E., and Choudhari, M., "Unsteady Flow Computation of a Slat with a Blunt Trailing Edge," *AIAA Journal*, Vol. 38, No. 11, 2000, pp. 2050–2058.

[23]Meadows, K. R., Brooks, T. F., Humphreys, W. M., Hunter, W. H., and Gerhold, C. H., "Aeroacoustic Measurements of a Wing-Flap Configuration," AIAA Paper 97-1595, May 1997.

[24]Thies, A. T., and Tam, C. K. W., "Computation of Turbulent Axisymmetric and Nonaxisymmetruc Jet Flows Using the k–ε Model," *AIAA Journal*, Vol. 34, No. 2, 1996, pp. 309–316.

[25]Tam, C. K. W., and Dong, Z., "Wall Boundary Conditions for High-Order Finite Difference Schemes in Computational Aeroacoustics," *Theoretical and Computational Fluid Dynamics*, Vol. 8, Oct. 1994, pp. 303–322.

[26]Tam, C. K. W., Webb, J. C., and Dong, Z., "A Study of the Short Wave Components in Computation Acoustics," *Journal of Computational Acoustics*, Vol. 1, March 1993, pp. 1–30.

[27]Khorrami, M. R., Berkman, M. E., Choudhari, M., Singer, B. A., Lockard, D. P., and Brentner, K. S., "Unsteady Flow Computations of a Slat with a Blunt Trailing Edge," AIAA Paper 99-1805, May 1999.

[28]Storms, B. L., Ross, J. C., Horne, W. C., Hayes, J. A., Dougherty, R. P., Underbrink, J. R., Scharpf, D. F., and Moriarty, P. J., "An Aeroacoustic Study of an Unswept Wing with a Three Dimensional High-Lift System," NASA TM-1998-112222, 1998.

M. Samimy
Associate Editor